Results

Fig. 4.19 shows the final 2D depth sections obtained from stacking scheme 2 and scheme 5. Both are 60 km deep and 100 km wide, starting 30 km west of the coast and ending 70 km east of it.

The top section was obtained by stacking the absolute amplitudes of the single migrated sections. The section shows a strong east dipping reflector between $x = $ -20 km and $x = $ -15 km at depths between 15 - 20 km. A thicker almost horizontal reflector is visible at 20 km depth between $x = $ -15 km and 0 km. In the middle of the profile ($x = $ 0 - 22 km) two parallel 5 km thick east dipping reflection bands are visible. The upper reflection band becomes horizontal between $x = $ 22 - 32 km and is located at depths between 14 - 16 km. The shape of the lower band at a depth of 22 km between $x = $ 19 - 30 km becomes diffuse and weak. Between $x = $ 12.5 - 17.5 km at depths between 25 - 28 km a thin east dipping reflector is visible. The reflectors at larger depths become unpronounced and indistinct. In the eastern part of the profile between $x = $ 45 - 55 km at depths between 10 - 13 km slightly west dipping reflectors are visible. Below, at a depth of 22 km a thin horizontal reflector is visible between $x = $ 42 - 49 km. The west dipping and slightly curved reflectors visible at depths larger than 30 km between $x = $ 40 - 70 km are migration artefacts. The strong reflectors at the beginning and in the middle of the profile are interpreted as the permotriassic accretionary wedge. Reflections neither from the continental Moho nor from the oceanic crust are recognised in the section. The weak appearance of the reflectors at depths larger than 30 km in the middle of the profile is assumed to be caused by the amplitude and coherency loss due to scattering in the highly heterogeneous and complex overburden as well as the low data coverage.

The lower section in Fig. 4.19 shows the depth section obtained by envelope stacking and additional normalisation of the section to the maximum amplitudes of each depth trace. The amplitude amplification provided an image where deeper structures appear more pronounced. The east dipping reflector at the beginning of the profile (between $x = $ -20 km and $x = $ -15 km) is sharp and clearly visible. Between $x = $ -10 km and 0 km thin horizontal reflectors are visible. The thick parallel east dipping reflection bands at depths between 5 - 22 km in the middle of the profile ($x = $ 0 - 25 km) appear weaker and less pronounced than in the other final section (Fig. 4.19, top). Below, at depths larger than 25 km, a number of east dipping thin reflectors are clearly visible. Between $x = $ 17.5 - 52.5 km a band of horizontal reflectors is visible at a depth of 22 km. The reflection strength and the coherency change along the reflection band. The most coherent reflectors are visible in the eastern part of the section ($x = $ 40 - 50 km). The migration
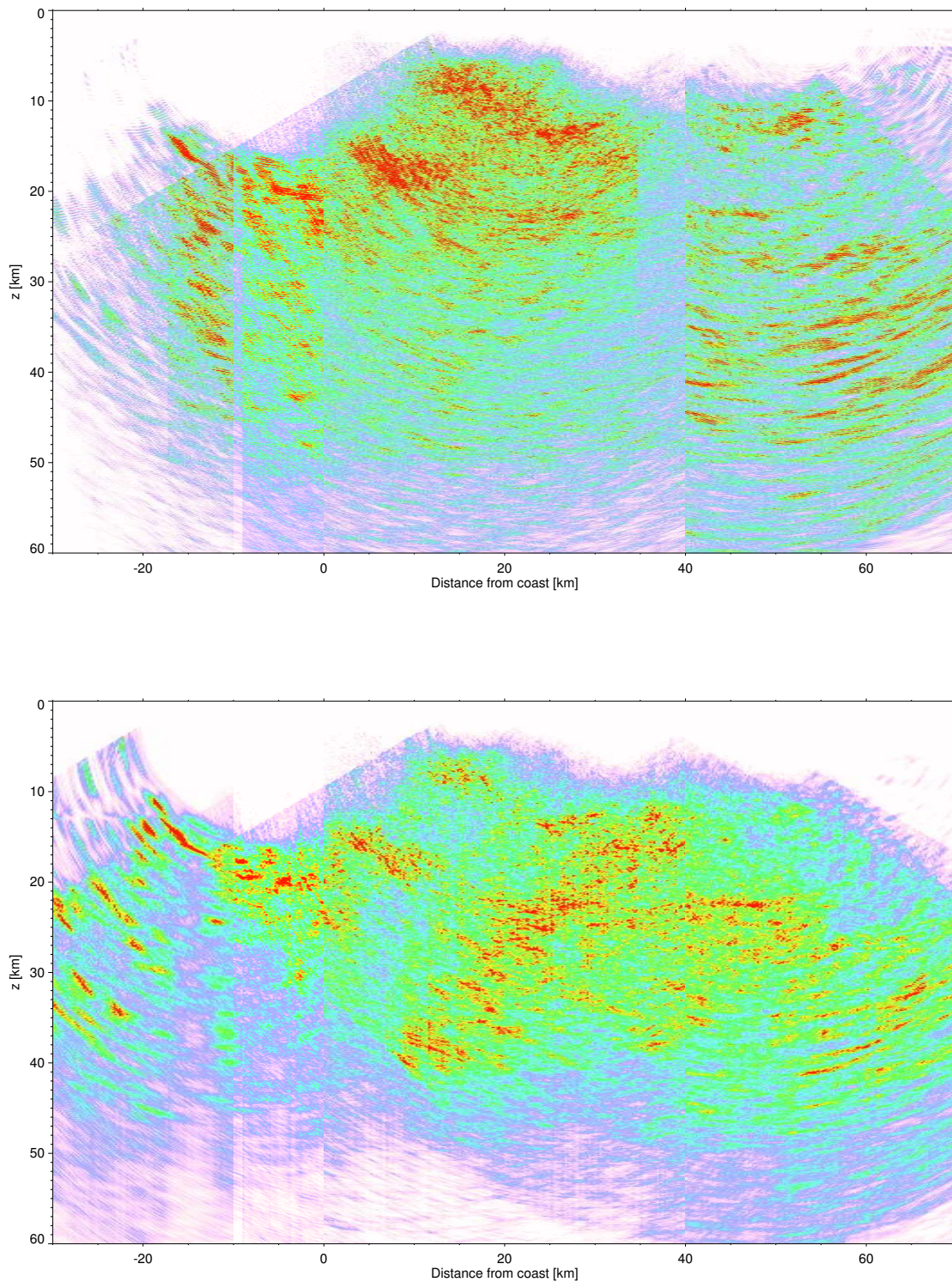
Figure 4.19: **Top :** Depth section obtained by stacking scheme 2. **Bottom :** Depth section obtained by stacking scheme 5.

noise in the eastern part of the profile appears less strong than in the top section Fig. 4.19.

In Fig. 4.20 the normalised depth section is displayed with the hypocenter locations between $38° - 38°25$ S (Bohm et al., 2002). Also, prominent reflectors derived from the wide-angle data are displayed. Contrary to the images from the Central Andes the hypocenter locations provide no indication on the geometry of the oceanic plate. According to the compilation all hypocenters are located in the continental crust. Interestingly, the east dipping reflections at depths between 30 - 35 km and 35 - 40 km in the middle of the profile almost correlate with the position of the oceanic crust derived from the wide-angle data. The upper reflections at depths between 30 - 35 km are interpreted as the boundary between the continental and the oceanic crust, the lower ones (35 - 40 km) as the reflections from the oceanic Moho. The reflections in the middle of the profile match well with the wide-angle reflector in the continental crust at depths around 23 km. These are interpreted as the Conrad discontinuity, which are located between the upper and the lower continental crust.

4.3.3   RIS applied to SPOC-NVR

The depth sections presented in the previous section provided weak evidence for the location of the oceanic crust. In order to reveal deeper reflectors that suffered from amplitude and coherency loss due to scattering in the heterogeneous continental mantle the depth sections were recalculated using narrow frequency bands of the data set (RIS).

The RIS method was applied in the same way as for the ANCORP data (see section 4.2.4). The shot gathers were band-pass filtered and migrated in three frequency bands (5 - 10 Hz, 10 - 15 Hz, and 15 - 20 Hz). The migration of the filtered data and the stacking of the migrated sections were carried out exactly in the same way as for the unfiltered data (described in section 4.3.2). Again, a comparison of differently stacked sections showed that the section obtained from stacking scheme 5 provided the most detailed reflection image. These results will be presented and discussed in the following. The filtered depth sections obtained from stacking scheme 2 are given in appendix B.

Results

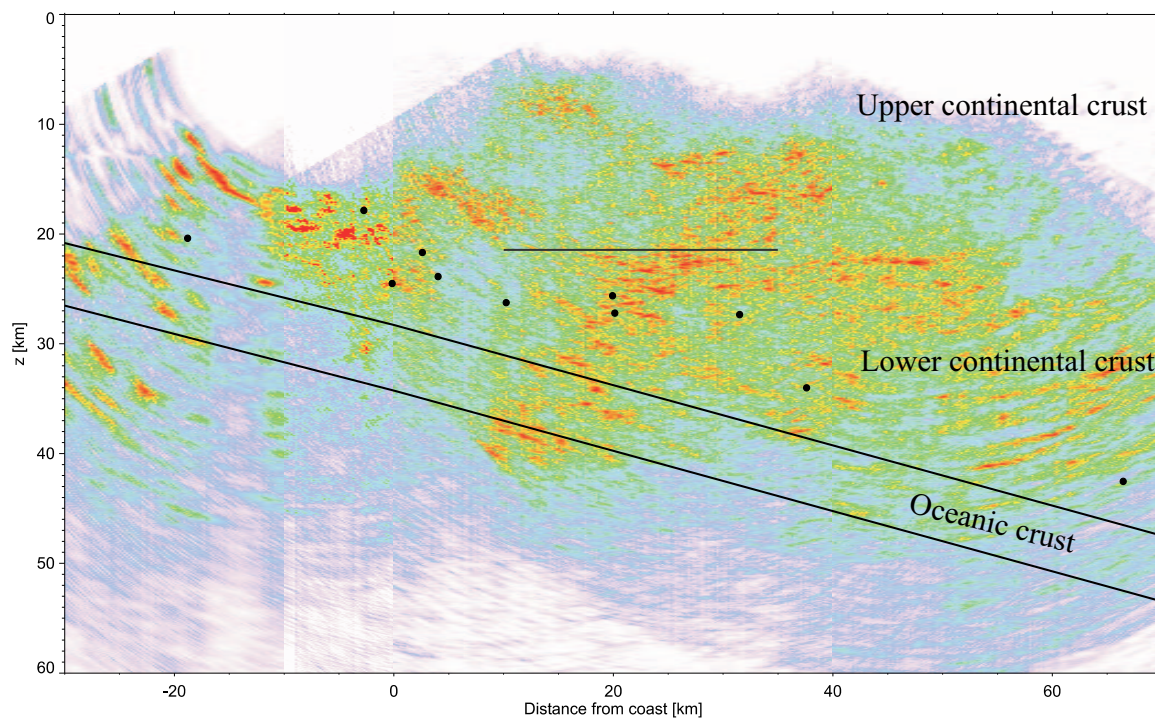All sections are displayed using the same amplitude scaling.

Figure 4.20: Trace normalised section of envelope stack with ISSA hypocenters between $38° - 38°25$ S (after Bohm et al. (2002)). The black lines indicate prominent wide-angle reflectors derived from refraction data analysis (Lüth et al., 2003a). In the middle of the profile the east dipping reflectors at depths between 35 - 40 km correlate well with the position of the oceanic Moho. Also, the reflectors visible in the middle of the profile at depths around 23 km match well with the boundary between the upper and the lower continental crust (Conrad discontinuity).
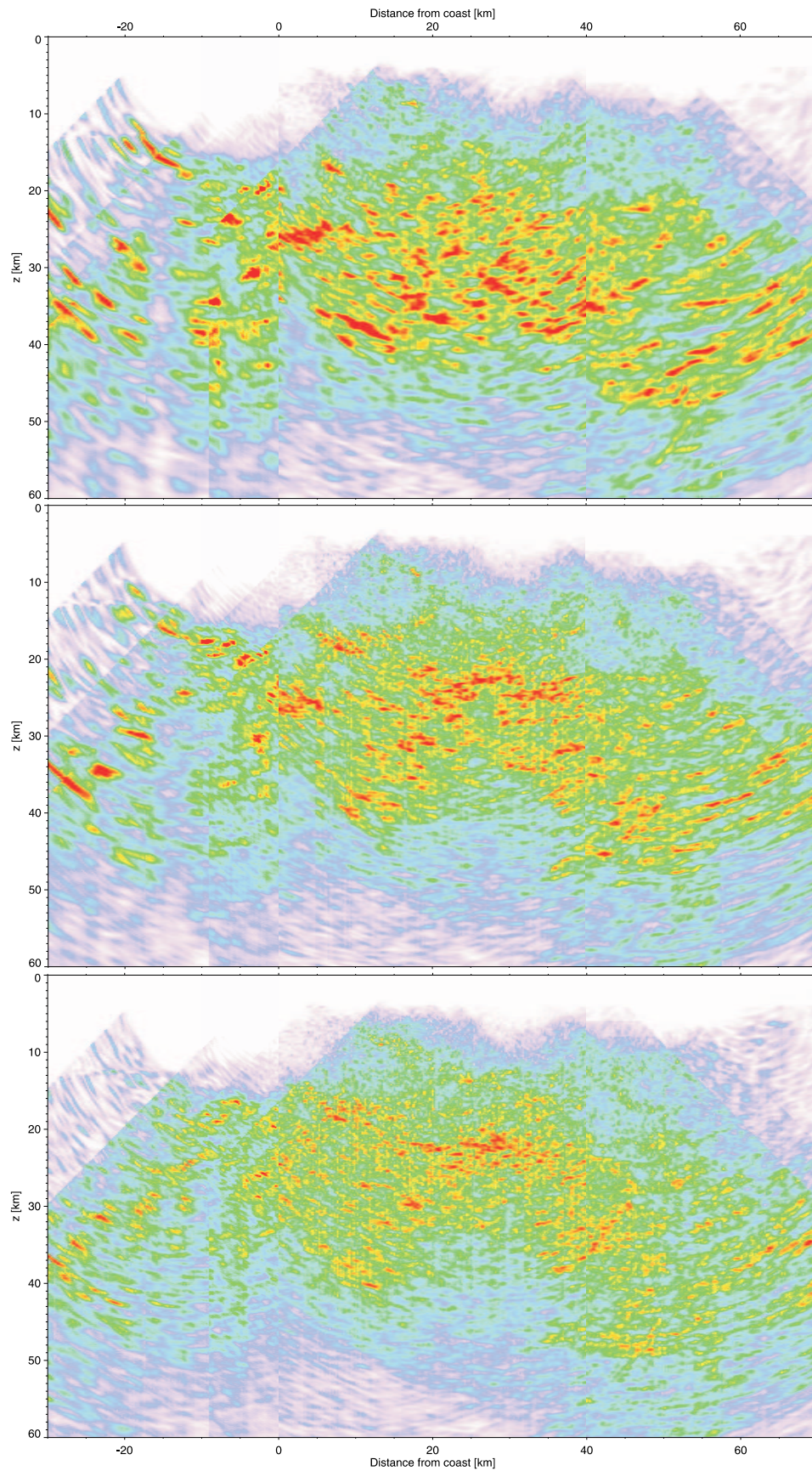
Figure 4.21: **Top:** Low-frequency image (5 - 10 Hz). **Middle:** Intermediate-frequency image (10 - 15 Hz). **Bottom:** High-frequency image (15 - 20 Hz).

The top section in Fig. 4.21 shows the low-frequency section (5 - 10 Hz). The dominant wavelengths are 500 - 1000 m ($v_P = 5000$ ms^{-1}). The normal-incidence Fresnel zone widths at a depth of 20 km are 4500 - 6400 m, and at a depth of 40 km 6300 - 9000 m, respectively. The thin dipping reflector at the beginning of the profile (between $x = -20$ km and $x = -15$ km) is clearly visible. A thick and slightly west dipping reflector is visible at depths between 24 - 27 km ($x = 0 - 8$ km). This reflector was not pronounced in the unfiltered section. The reflections at depths between 20 - 35 km appear diffuse and incoherent between $x = 5 - 40$ km. In the middle of the profile at depths larger than 30 km a number of east dipping reflections are visible. Among these a strong and east dipping reflection is pronounced between 5 - 15 km at depths between 35 - 40 km. This reflection correlates well with the oceanic Moho observed in the wide-angle data.

The intermediate-frequency section is shown in the middle of Fig. 4.21. The dominant wavelengths are 333 - 500 m. The normal-incidence Fresnel zone widths at a depth of 20 km are 3700 - 4500 m, and at a depth of 40 km 5000 - 6300 m, respectively. The section shows thin dipping reflections between $x = -20$ km and $x = -15$ km that appear less pronounced compared with the unfiltered or the low-frequency image. Between $x = -15$ km $x = -5$ km the reflections appear almost horizontal at a depth of around 17 km. Bands of east dipping reflections are visible between $x = 0 - 5$ km at depths between 24 - 27 km and between $x = 5 - 12$ km at depths between 17 - 20 km. Further to the east ($x = 20 - 40$ km) horizontal and slightly west dipping reflections are visible at depths between 20 - 27 km. In the lower part of the image (25 km $\leq$ z) parallel bands of east dipping reflections are visible in the middle of the profile ($x = 0 - 40$ km).

The high frequency image is shown in the bottom of Fig. 4.21. The dominant wavelengths are 250 - 333 m. The normal-incidence Fresnel zone widths at a depth of 20 km are 3200 - 3600 m, and at a depth of 40 km 4500 - 5100 m, respectively. The reflections appear weaker and incoherent compared to the low- and the intermediate-frequency section. Between $x = 5 - 15$ km thin east dipping reflections are visible at depths between 17 - 23 km. These reflections merge with a band of thin parallel horizontal reflections between $x = 15 - 35$ km at a depth of around 23 km. Weak east dipping reflections at depths between 25 - 40 km are visible between $x = 0 - 20$ km.

The reflections from the continental crust appear differently pronounced in the recalculated images. The low-frequency and the intermediate-frequency image clearly show east dipping reflections at the beginning of the profile (between $x = -20$ km and $x = -10$ km). These reflections do not appear in the high-frequency image. Thick and apparently west dipping reflections at depths between 24 - 27 km between $x = 0 - 8$ km are visible in the low-

frequency image, while in the intermediate-frequency image the same reflections appear as weaker thin reflections with an apparent east dipping component. These reflections do not appear in the high-frequency image. In the intermediate-frequency image slightly west dipping reflections between $x = 20$ - 32 km at depths between 22 - 26 km and a ca. 1 km thick band of mainly horizontal reflections is visible between $x = 28$ - 39 km. In the high-frequency image these reflections appear as a band of short horizontal reflections with varying thickness (2 - 4 km). The reflections from the oceanic crust are pronounced strongest in the low-frequency image. There, a strong east dipping reflection in the middle of the profile ($x = 5$ - 15 km) is clearly visible at depths between 35 - 40 km. This reflection is interpreted as the oceanic Moho. These reflections are only weakly visible in the intermediate- and in the high-frequency image.

The application of RIS to the NVR data set does not provide additional details to the structures visible in the envelope stacked and trace normalised section (Fig. 4.19, bottom). The filtered sections reveal reflections from the complex fabric of the permotriassic accretionary wedge, which are also visible in the unfiltered image. However, the low-frequency image provides clearly pronounced reflections from the oceanic Moho, that appeare less pronounced in the unfiltered image. Thus, in the case of the NVR data the recalculated images contribute only slightly to an improved structural interpretation.

4.4 Summary

In this chapter the deep reflection data sets ANCORP, PRECORP and SPOC-NVR were processed. Kirchhoff prestack depth migration of the ANCORP data using three different velocity models and the application of the RIS method to the data provided new insight into subduction zone of the Central Andes. The prestack depth migration and the application of the RIS method to the NVR-SPOC data revealed structural details from the Southern Andes.

The prestack depth migrated images of the ANCORP ($21°$ S) and the PRECORP data ($22.5°$ S) provide structural images of an erosive margin type subduction zone. An analysis of the 3D ANCORP depth volume revealed an additional north dipping component of the west dipping QBBS. This observation and the image of the CBS in the PRECORP section indicate that both bright spots are related to the same structure or the same origin. A compilation of parts from both depth sections showed that the depth and the geometry of the subducting oceanic plate does almost not change over a distance of 160 km in N-S-direction. In both sections an apparent offset between the Nazca reflector and the

hypocenter locations is observed. This offset indicates that the Nazca reflector reflects a strongly reflective zone above the oceanic crust rather than marking the top of the oceanic crust.

To study whether the observed offset is a result of using an improper velocity model for migration or a real offset related to the subsurface structure, the ANCORP data were remigrated using two alternative velocity models from tomographic inversion. An analysis of travel times calculated for the velocity models showed that both tomography models differed significantly from each other and from the refraction data model. A comparison of the recalculated images showed that the refraction model provides an accurate image of the reflections from the oceanic crust in the beginning of the profile as well as of the deeper Nazca reflector. In both other images either the reflections from the top and bottom of the oceanic crust ($x = 0$ - 50 km) are not imaged properly in depths or the image of the Nazca reflector appears distorted and diffuse. The compilation of the recalculated images with the hypocenters showed that the apparent offset between the top of the hypocenters and the Nazca reflector remains, independent from the velocity model used for migration.

Also, the RIS method was applied the ANCORP data to extract additional structural details. The sections were calculated for narrow frequency bands of the data (5 - 10 Hz; 10 - 15 Hz; 15 - 20 Hz) and analysed. The images provide distinct reflections interpreted as the top and bottom of the oceanic crust along the first 110 km of the profile for all frequency ranges. In the middle of the profile the high-frequency image (15 - 20 Hz) reveals thin east dipping reflections that are not observed in the image calculated for the whole frequency range. From these reflections direct indication is given that the top of the oceanic crust is located near the lower boundary of the Nazca reflector. The position correlates with the prolongation of the oceanic crust, visible along the first 70 km of the section, into larger depths. Also, thin horizontal reflections are visible, which are interpreted as the top of the hydrated continental mantle wedge.

In the last part of this chapter the prestack depth migration was applied to the SPOC-NVR data from the Southern Andes at 38° S. The implementation of e different stacking schemes provided structural details of the permotriassic accretionary wedge and of the oceanic crust at depths down to 40 km. A good correlation was observed between the reflections from the continental and oceanic crust and the wide-angle reflectors observed from refraction data analysis (Lüth et al., 2003a). For example the boundary between the upper and the lower continental crust was observed at similar depths in both data. The application of RIS to the NVR data recovered a pronounced reflection from the oceanic Moho at depths between 35 - 40 km. However, additional details on the structure

within the continental crust were not obtained. It is assumed that the NVR data are very sensitive to the stacking scheme and to the amplitude enhancement processing due to its low coverage and the low signal-to-noise ratio.

The results from the application of the RIS method to the ANCORP and the SPOC-NVR data show that the method is an appropriate tool to recover and to extract reflections that are less pronounced in the unfiltered image. Especially in areas where scattering becomes dominant, deeper structures can be recovered by imaging only narrow-frequency bands. Thus, the structural interpretation of seismic data is improved. However, the efficiency of the method appears to be strongly dependent on the data coverage, the data quality and the subsurface structures that are investigated.